The Aeronautical Journal (2024), **128**, pp. 2126–2147
doi:10.1017/aer.2024.4

RESEARCH ARTICLE

Finite-time attitude tracking control of stratospheric airship in the presence of multiple disturbances

Z.B. Li , D.P. He, J.Q. Zhang and X.R. Meng

School of Electrical Engineering and Automation, Shandong University of Science and Technology, Qingdao, China
Corresponding author: D.P. He; Email: 17860281617@163.com

Received: 5 September 2023; **Revised:** 11 November 2023; **Accepted:** 8 January 2024

Keywords: stratospheric airship; attitude tracking; reduced-order extended state observer; composite non-singular fast terminal sliding mode

Abstract

This paper proposes a composite non-singular fast terminal sliding mode attitude control scheme based on a reduced-order extended state observer for the stratospheric airship's attitude system affected by multiple disturbances. First, the feedback linearisation method is applied to address the nonlinearity of the attitude motion model and achieve decoupling of the model in three channels. Second, the overall disturbances, encompassing airship parameter perturbations and external disturbances, are treated as an aggregate. A reduced-order extended state observer is designed for each channel to formulate a composite non-singular fast terminal sliding mode surface. In the control design phase, the hyperbolic sine function is adopted as replacement for the sign function to ensure the continuity of the control signal. The estimated disturbances are incorporated in the control law design to directly offset the effects of multiple disturbances on the attitude motion of the airship. Third, based on Lyapunov theory, it has been proven that the control law can drive the attitude tracking error to converge to zero within a finite time. Simulation results demonstrate that the proposed control scheme exhibits favorable disturbance rejection capability, as well as higher tracking accuracy and faster response speed.

Nomenclature

RESO	reduced-order extended state observer
CNFTSMC	composite non-singular fast terminal sliding mode controller
NFTSMC	non-singular fast terminal sliding mode controller

1.0 Introduction

As scientific and technological advances rapidly progress, the remarkable applicability of near-space vehicles is increasingly prominent. Among these, stratospheric airship, characterised by low energy consumption, high cost-effectiveness, prolonged flight duration and substantial payload capacity, is extensively utilised in a range of applications such as regional warning, environmental monitoring, communication relay, regional navigation and emergency response [1]. Stratospheric airship adjusts the attitude to track specific trajectories and execute flight missions, thus high-precision and robust finite-time attitude tracking control is pivotal in the design of stratospheric airship flight control system [2, 3]. However, the attitude dynamic model of stratospheric airship exhibits high nonlinearity and strong channel coupling [4], posing significant challenges to control system design. In addition, model parameter perturbations and complex flight environment [5, 6] considerably impact the attitude tracking accuracy of stratospheric airship.

In addressing the challenges encountered in airship attitude control, researchers have undertaken various studies. Reference (7) designed the attitude control system of the airship based on fault-tolerant backstepping control law, facilitating the tracking of desired attitude with robustness to step bias and time-varying bias. Reference (8) developed a full-state feedback controller for airship based on the linear quadratic gaussian/loop transfer recovery algorithm to control the horizontal attitude angle of the airship under wind disturbances. Reference (9) devised a self-disturbance attitude tracking controller for the pitch angle and yaw angle of the airship affected by wind field disturbances.

Sliding mode control has prominent advantages such as a simple structure and robustness [10, 11], and has been extensively utilised in the design of aircraft control system. In Ref. [12], a terminal sliding mode control method was employed to design an attitude tracking control law, achieving convergence of the attitude tracking error to zero within a finite time. However, the introduced external disturbance torque was deemed insufficient to demonstrate the disturbance rejection capability of the proposed control algorithm. During the modeling process, multiple disturbances such as parameter perturbations and external disturbances caused by complex environment were identified, making it difficult to achieve rapid disturbances suppression relying on the robustness of the control algorithm itself. By designing an extended state observer [13], the total disturbances of the system were regarded as the new state variable, with the disturbances estimation values incorporated into the controller design in the form of feedforward [14] to directly suppress the effects of disturbances. Reference (15) employed a traditional nonlinear extended state observer to estimate the total disturbances, with the resulting disturbances estimation information integrated into the design of the terminal sliding mode controller to mitigate the influence of parameter perturbations and external disturbances, thus achieving the desired attitude tracking of the airship. However, in the simulation experiments conducted in Ref. [15], the chosen model mass and moment of inertia of the airship were too large, resulting in limited changes in attitude angles and requiring a substantial control torque, which may exceed the upper limit of the control torque provided by the actual actuator. Taking into account the limitation of the control torque, it is vital to meticulously design and select parameters for the control system to ensure its alignment with the control requirements of the actual actuator. It is worth noting that the traditional nonlinear extended state observer is susceptible to causing phase lag in the system, and the magnitude of the phase lag amplifies with the increasing order of the nonlinear extended state observer. One effective method to address this issue is to reduce the order of the nonlinear extended state observer, namely using a reduced-order extended state observer [16].

This paper addresses the attitude tracking problem of stratospheric airship under the influence of external disturbances and parameter perturbations. It proposes a composite non-singular fast terminal sliding mode attitude control scheme based on a reduced-order extended state observer. Firstly, the mathematical model of the airship's attitude motion is established, and the input-output feedback linearisation is utilised to decompose the nonlinear attitude motion system into three-channel subsystems. Subsequently, a reduced-order extended state observer is designed to estimate and compensate for the total disturbances of the system. Based on the disturbances estimation information and the composite non-singular fast terminal sliding mode control algorithm, a composite non-singular fast terminal sliding mode controller based on the reduced-order extended state observer is designed. Finally, the effectiveness of the proposed method is verified through simulation.

This paper makes the following contributions:

(1) In comparison to the work presented in Ref. [15], this paper introduces a reduced-order extended state observer that effectively mitigates the phase lag caused by the observer. By estimating real-time system disturbances with smaller gains and a simplified structure, the proposed observer significantly enhances the robustness of the attitude system against multiple disturbances.

(2) In the design of the control scheme, this paper proposes a novel composite sliding surface based on the tracking error performance function. Unlike the integral sliding mode employed in Ref. [17], the proposed composite sliding surface provides superior sliding trajectory for the state variable, resulting in faster and more accurate tracking of the desired attitude angles.

https://doi.org/10.1017/aer.2024.4 Published online by Cambridge University Press

(3) Diverging from existing findings in Ref. [18], this paper introduces the hyperbolic sine function as a replacement for the sign function in the control law design, eliminating the chattering phenomenon of sliding mode while ensuring the continuity of control signals.

These contributions substantiate the effectiveness and superiority of the adopted composite nonsingular fast terminal sliding mode attitude control scheme in this study. The proposed method enables rapid and accurate tracking control of stratospheric airship attitude in complex environment with multiple disturbances, thus contributing to the advancement of practical applications for stratospheric airship.

2.0 Preliminaries and problem statement

2.1 Preliminaries

Consider the following system [19]:

$$\dot{\lambda}(t) = f(\lambda(t)), \lambda(0) = \lambda_0 \tag{1}$$

where $\lambda = \left[\lambda_1, \lambda_2, \ldots, \lambda_n\right]^{\mathrm{T}}$, $f(\cdot)$ is a continuous nonlinear function, assuming the origin is an equilibrium point for system (1).

Lemma 1. *If there exists a Lyapunov function V, such that* $\dot{V} \le -\mu_1 V - \mu_2 V^{n_1}$, $\mu_1 > 0$, $\mu_2 > 0$ *and* $0 < n_1 < 1$, *then the system (1) is finite-time stable at the origin, and V converges to 0 within a finite time [20].*

$$\mathrm{T} \le \frac{1}{\mu_1 (1 - n_1)} \ln \frac{\mu_1 V^{1-n_1}(0) + \mu_2}{\mu_2} \tag{2}$$

Lemma 2. *If there exists a Lyapunov function V, such that* $\dot{V} \le -\mu_1 V^{n_1}$, $\mu_1 > 0$ *and* $0 < n_1 < 1$, *then the system (1) is finite-time stable at the origin, and V converges to 0 within a finite time [21].*

$$\mathrm{T} \le \frac{V^{1-n_1}(0)}{\mu_1 (1 - n_1)} \tag{3}$$

2.2 Problem statement

According to Ref. [22], the six degrees of freedom kinematic equation for an airship is given by

$$\begin{pmatrix} P \\ \Omega \end{pmatrix} = \begin{pmatrix} R_1 & 0_{3\times3} \\ 0_{3\times3} & R_2 \end{pmatrix} \begin{pmatrix} V \\ W \end{pmatrix} \tag{4}$$

where $P = \left[x, y, z\right]^T$, $\Omega = [\theta, \psi, \phi]^T$, $V = [u, v, w]^T$, $W = \left[p, q, r\right]^T$,

$$R_1 = \begin{bmatrix} \cos\psi\cos\theta & \cos\psi\sin\theta\sin\phi - \sin\psi\cos\phi & \cos\psi\sin\theta\cos\phi + \sin\psi\sin\phi \\ \sin\psi\cos\theta & \sin\psi\sin\theta\sin\phi + \cos\psi\cos\phi & \sin\psi\sin\theta\cos\phi - \cos\psi\sin\phi \\ -\sin\theta & \cos\theta\sin\phi & \cos\theta\cos\phi \end{bmatrix},$$

$$R_2 = \begin{bmatrix} 0 & \cos\phi & -\sin\phi \\ 0 & \sec\theta\sin\phi & \sec\theta\cos\phi \\ 1 & \tan\theta\sin\phi & \tan\theta\cos\phi \end{bmatrix}.$$

x, y, and z are the airship's displacements along the longitudinal, lateral, and vertical axes; θ, ψ, and ϕ are the airship's pitch, yaw and roll angles; u, v and w are the velocity vector components along each axis; p, q and r are the airship's roll, pitch, and yaw angular velocities, respectively.

https://doi.org/10.1017/aer.2024.4 Published online by Cambridge University Press

Assuming the airship is a rigid body and neglecting its elastic deformation, the following ground-coordinate airship dynamic equation can be derived based on the Newton-Euler equation:

$$m\frac{dv_G}{dt} = F \tag{5}$$

$$v_G = v_o + \omega \times r_G \tag{6}$$

Upon substitution of Equations (6) into (5), we get

$$m\frac{dv_o}{dt} + m\frac{d\omega}{dt} \times r_G + m\omega \times \frac{dr_G}{dt} = F \tag{7}$$

where m is the airship's mass, v_G is the velocity vector of the centre of gravity, v_o is the velocity vector of the buoyancy centre, ω is the angular velocity vector, r_G is the vector from the buoyancy centre to the centre of gravity, and F is the force acting on the airship.

$$\frac{dH}{dt} = \tau \tag{8}$$

$$H = I_o\omega + r_G \times (mv_o) \tag{9}$$

Upon substitution of Equations (9) into (8), we obtain

$$\begin{bmatrix} mE_{3\times3} & -mr_G^{\times} \\ mr_G^{\times} & I_o \end{bmatrix}\begin{bmatrix} \dot{v}_o \\ \dot{\omega} \end{bmatrix} + \begin{bmatrix} m\omega^{\times}\dot{v}_o + m\omega^{\times}(\omega^{\times}r_G) \\ \omega^{\times}(I_o\omega) + mr_G^{\times}(\omega^{\times}v_o) \end{bmatrix} = \begin{bmatrix} F \\ \tau \end{bmatrix} \tag{10}$$

where H is the moment of force relative to the buoyancy centre, I_o is the moment of inertia matrix relative to the buoyancy centre, and τ is the moment of force acting on the airship.

By the application of the vector derivative rule, the airship dynamic equation in the body coordinate system can be derived.

Based on Equation (7), we derive

$$m\frac{dv_o}{dt} + m\omega^{\times}v_o + m\frac{d\omega}{dt} \times r_G + m\omega^{\times}\left(\omega^{\times}r_G\right) = F \tag{11}$$

where $\omega^{\times}$ is the cross product matrix of the angular velocity vector ω.

From Equation (10), we have

$$I_o\frac{d\omega}{dt} + \omega^{\times}(I_o\omega) + m\left[r_G^{\times}\frac{dv_o}{dt} + \omega^{\times}\left(r_G^{\times}v_o\right)\right] = \tau \tag{12}$$

where $r_G^{\times}$ is the cross product matrix of the angular velocity vector r_G.

Combining Equations (11) and (12), we derive the matrix form of the dynamic equation

$$\begin{bmatrix} mE_{3\times3} & -mr_G^{\times} \\ mr_G^{\times} & I_o \end{bmatrix}\begin{bmatrix} \dot{v}_o \\ \dot{\omega} \end{bmatrix} + \begin{bmatrix} m\omega^{\times}\dot{v}_o + m\omega^{\times}(\omega^{\times}r_G) \\ \omega^{\times}(I_o\omega) + mr_G^{\times}(\omega^{\times}v_o) \end{bmatrix} = \begin{bmatrix} F \\ \tau \end{bmatrix} \tag{13}$$

If we account for the impact of additional mass and additional inertial force, the airship's dynamic equation can be formulated as

$$\begin{bmatrix} mE_{3\times3} + M_a & -mr_G^{\times} \\ mr_G^{\times} & I_o + I_a \end{bmatrix}\begin{bmatrix} \dot{v}_o \\ \dot{\omega} \end{bmatrix} + \begin{bmatrix} (mE_{3\times3} + M_a)\left[\omega^{\times}\dot{v}_o + \omega^{\times}(\omega^{\times}r_G)\right] \\ \omega^{\times}\left[(I_o + I_a)\,\omega\right] + mr_G^{\times}(\omega^{\times}v_o) \end{bmatrix} = \begin{bmatrix} F \\ \tau \end{bmatrix} \tag{14}$$

where M_a and I_a are the additional mass matrix and additional moment of inertia matrix, respectively.

The attitude motion of the stratospheric airship in the geocentric reference frame ($O_bx_by_bz_b$) and the body reference frame ($O_ex_ey_ez_e$) is shown in Fig. 1. C_V is the buoyancy centre of the airship, while C_G is the centre of gravity. The vector from the buoyancy centre to the centre of gravity is denoted as $r_G = \left[x_G, y_G, z_G\right]^{\mathrm{T}}$.

https://doi.org/10.1017/aer.2024.4 Published online by Cambridge University Press

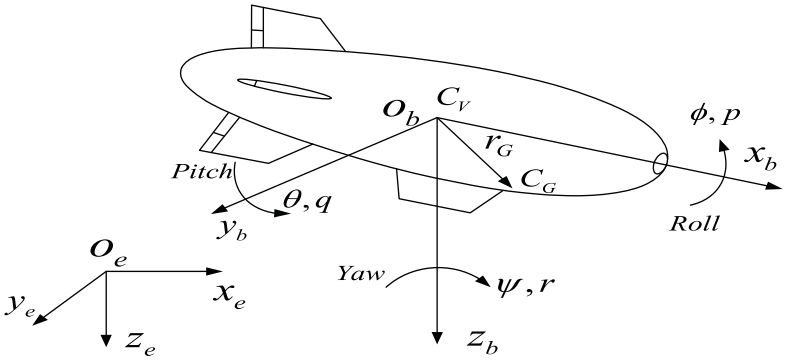

Figure 1. *Attitude motion diagram.*

From Equation (4) for the airship's kinematic Equation and Equation (14) for the airship's dynamic equation, we can obtain the mathematical model of the airship's attitude motion

$$\begin{bmatrix} \dot{\theta} \\ \dot{\psi} \\ \dot{\phi} \\ \dot{p} \\ \dot{q} \\ \dot{r} \end{bmatrix} = \begin{bmatrix} -r\sin\phi + q\cos\phi \\ \sec\theta\ (r\cos\phi + q\sin\phi) \\ p + \tan\theta\ (r\cos\phi + q\sin\phi) \\ (c_1 r + c_2 p)\ q + c_3\ (L - z_G G\cos\theta\sin\phi) + c_4 N \\ c_5 pr - c_6\left(p^2 - r^2\right) + c_7\ (M - z_G G\sin\theta) \\ (c_8 p + c_2 r)\ q + c_4\ (L - z_G G\cos\theta\sin\phi) + c_9 N \end{bmatrix}$$

where $c_1 = \frac{I_{xz}^2 - I_z(I_y - I_z)}{I_{xz}^2 - I_x I_z}$; $c_2 = -\frac{(I_x - I_y + I_z)I_{xz}}{I_{xz}^2 - I_x I_z}$; $c_3 = -\frac{I_z}{I_{xz}^2 - I_x I_z}$; $c_4 = -\frac{I_{xz}}{I_{xz}^2 - I_x I_z}$; $c_5 = \frac{I_z - I_x}{I_y}$; $c_6 = \frac{I_{xz}}{I_y}$; $c_7 = \frac{1}{I_y}$; $c_8 = \frac{I_x(I_y - I_x) - I_{xz}^2}{I_{xz}^2 - I_x I_z}$; $c_9 = -\frac{I_x}{I_{xz}^2 - I_x I_z}$; G is the gravity of the airship; L, M, N are the roll, pitch and yaw moments applied to the airship, respectively; I_x, I_y, I_z, and I_{xz} are the generalised moments of inertia.

During actual flight, the airship may be affected by external disturbances, and there may be some deviations in the model parameters. Let $I_{x1} = I_x + \Delta I_x$, $I_{y1} = I_y + \Delta I_y$, $I_{z1} = I_z + \Delta I_z$, and $I_{xz1} = I_{xz} + \Delta I_{xz}$. Where ΔI_x, ΔI_y, ΔI_z, and ΔI_{xz} are the uncertain parts of the moments of inertia.

By selecting the state variable $x = [\theta, \psi, \phi, p, q, r]^T$, control variable $u = [-I_z L - I_{xz} N, M, -I_{xz} L - I_x N]^T$, output variable $h(x) = [\theta, \psi, \phi]^T$ and external disturbance torque $d = [d_1, d_2, d_3]^T$, the mathematical model of the airship attitude motion system can be described as the following nonlinear system

$$\begin{cases} \dot{x} = (f(x) + \Delta f(x)) + (g(x) + \Delta g(x))\, u + T \\ y = h(x) \end{cases} \tag{15}$$

where

$$f(x) = \begin{bmatrix} -r\sin\phi + q\cos\phi \\ \sec\theta\ (r\cos\phi + q\sin\phi) \\ p + \tan\theta\ (r\cos\phi + q\sin\phi) \\ (c_1 r + c_2 p)\ q - c_3 z_G G\cos\theta\sin\phi \\ c_5 pr - c_6\left(p^2 - r^2\right) - c_7 z_G G\sin\theta \\ (c_8 p + c_2 r)\ q - c_4 z_G G\cos\theta\sin\phi \end{bmatrix},$$

https://doi.org/10.1017/aer.2024.4 Published online by Cambridge University Press

$$g(x)=\begin{bmatrix}0 & 0 & 0\\ 0 & 0 & 0\\ 0 & 0 & 0\\ 1/-I_xI_z+I_{xz}^2 & 0 & 0\\ 0 & 1/I_y & 0\\ 0 & 0 & 1/-I_xI_z+I_{xz}^2\end{bmatrix},$$

$$T=\begin{bmatrix}0\\ 0\\ 0\\ d_1/-I_xI_z+I_{x\Xi}^2\\ d_2/I_y\\ d_3/-I_xI_z+I_{x\Xi}^2\end{bmatrix},\ \Delta f(x)=\begin{bmatrix}0\\ 0\\ 0\\ ((c_{11}-c_1)r+(c_{22}-c_2p))q-(c_{33}-c_3)z_GG\cos\theta\sin\phi\\ (c_{55}-c_5)pr-(c_{66}-c_6)\left(p^2-r^2\right)-(c_{77}-c_7)z_GG\sin\theta\\ ((c_{88}-c_8)p+(c_{22}-c_2)r)q-(c_{44}-c_4)z_GG\cos\theta\sin\phi\end{bmatrix},$$

$$\Delta g(x)=\begin{bmatrix}0 & 0 & 0\\ 0 & 0 & 0\\ 0 & 0 & 0\\ 1/-I_{x1}I_{z1}+I_{x1}^2-1/-I_xI_z+I_{z2}^2 & 0 & 0\\ 0 & 1/I_{y1}-1/I_y & 0\\ 0 & 0 & 1/-I_{x1}I_{z1}+I_{z1}^2-1/-I_xI_z+I_{zz}^2\end{bmatrix}.$$

where $c_{11}=\frac{I_{xz1}^2-I_{z1}\left(I_{y1}-I_{z1}\right)}{I_{xz1}^2-I_{x1}I_{z1}}$; $c_{22}=-\frac{\left(I_{x1}-I_{y1}+I_{z1}\right)I_{xz1}}{I_{xz1}^2-I_{x1}I_{z1}}$; $c_{33}=-\frac{I_{z1}}{I_{xz1}^2-I_{x1}I_{z1}}$; $c_4=-\frac{I_{xz1}}{I_{xz1}^2-I_{x}1I_{z}1}$; $c_5=\frac{I_{z1}-I_{x1}}{I_{y1}}$; $c_6=\frac{I_{xz1}}{I_{y1}}$; $c_7=\frac{1}{I_{y1}}$; $c_8=\frac{I_{x1}\left(I_{y1}-I_{x1}\right)-I_{xz1}^2}{I_{xz1}^2-I_{x1}I_{z1}}$.

According to Ref. [17], the nonlinear attitude system can be transformed into the following system through coordinate transformation and state feedback

$$\begin{cases}\dot{\xi}=A\xi+B(v+f)\\ y=C\xi\end{cases}\tag{16}$$

where $v=[v_1,v_2,v_3]^T$ represents the pseudo-control variable; $f=[f_1,f_2,f_3]^T$ accounts for system parameter perturbations and external disturbances; y denotes the system output; ξ, A, B and C are given by

$$\xi=\begin{pmatrix}\xi_1\\ \xi_2\\ \xi_3\\ \xi_4\\ \xi_4\\ \xi_5\\ \xi_6\end{pmatrix}=\begin{pmatrix}\theta\\ -r\sin\phi+q\cos\phi\\ \psi\\ \frac{1}{\cos\theta}(r\cos\phi+q\sin\phi)\\ \phi\\ p+\tan\theta(r\cos\phi+q\sin\phi)\end{pmatrix},\ A=\begin{pmatrix}0&1&0&0&0&0\\ 0&0&0&0&0&0\\ 0&0&0&1&0&0\\ 0&0&0&0&0&0\\ 0&0&0&0&0&1\\ 0&0&0&0&0&0\end{pmatrix},\ B=\begin{pmatrix}0&0&0\\ 1&0&0\\ 0&0&0\\ 0&1&0\\ 0&0&0\\ 0&0&1\end{pmatrix},$$

https://doi.org/10.1017/aer.2024.4 Published online by Cambridge University Press

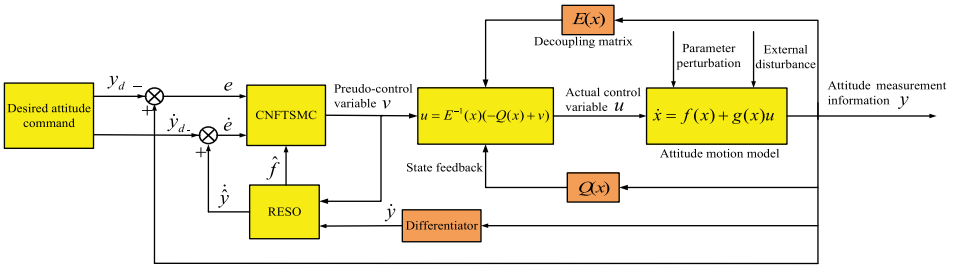

Figure 2. *Structure diagram of the attitude control system.*

$$C = \begin{pmatrix} 1 & 0 & 0 & 0 & 0 & 0 \\ 0 & 0 & 1 & 0 & 0 & 0 \\ 0 & 0 & 0 & 0 & 1 & 0 \end{pmatrix}$$

Remark 1. The pseudo control signal is the output of the subsequent controller in the following section. The correspondence between the pseudo control signal and the actual control signal can be expressed through feedback, represented by $u = E^{-1}(x)(-Q(x) + v)$, where $E(x)$ and $Q(x)$ are presented in Ref. [17]. By selecting an appropriate pseudo control signal and integrating it with feedback, finite time [23] tracking control of the system output variable can be achieved.

Remark 2. In the course of airship flight, it is exposed to external disturbances such as wind fields, which can deteriorate the precision of the controller. Owing to current technological constraints, obtaining real-time measurements of wind disturbances is challenging. Additionally, the substantial size of the airship makes it arduous to achieve precise measurement of the model parameters. In the subsequent section, an observer will be designed to estimate f, without relying on additional sensors.

3.0 Controller design

In this section, we will initially formulate the Reduced-order Extended State Observer (RESO) for each of the three channels to accomplish real-time estimation and compensation of multiple disturbances. Subsequently, leveraging the estimation information, we will proceed to devise the Composite Nonsingular Fast Terminal Sliding Mode Controller (CNFTSMC) employing the RESO for each channel, with the objective of attaining high-precision tracking of the airship's attitude in a multi-disturbance environment. The structure diagram of the attitude control system is illustrated in Fig. 2.

3.1 Design of the RESO

The design of the RESO is exemplified using the pitch angle channel as an example, with similar design method applied to the other channels. Based on Equation (16), the state space representation of the pitch angle channel can be formulated as

$$\begin{cases} \dot{\xi}_1 = \xi_2 \\ \dot{\xi}_2 = f_1 + v_1 \\ y_1 = \xi_1 \end{cases} \tag{17}$$

To accurately estimate the combined effect of parameter perturbations and external disturbances [24], define $\xi_7 = f_1$, and extend the state variables as $[\xi_1, \xi_2, \xi_7]^T$. Equation (17) can be rewritten as

https://doi.org/10.1017/aer.2024.4 Published online by Cambridge University Press

$$\begin{cases} \dot{\xi}_1 = \xi_2 \\ \dot{\xi}_2 = \xi_7 + \nu_1 \\ \dot{\xi}_7 = \dot{f}_1 \\ y_1 = \xi_1 \end{cases} \tag{18}$$

In Equation (18), the formulation of the traditional nonlinear extended state observer (ESO) is as follows:

$$\begin{cases} \dot{z}_1 = z_2 - b_1 fal_1\left(e_{E1}, a_1\right) \\ \dot{z}_2 = z_7 - b_2 fal_2\left(e_{E1}, a_2\right) + \nu_1 \\ \dot{z}_7 = -b_7 fal_7\left(e_{E1}, a_7\right) \end{cases} \tag{19}$$

where z_1 represents the estimated value of the output y_1, z_2 denotes the estimated value of the output derivative $\dot{y}_1$, z_7 signifies the estimated value of f_1, and e_{E1} pertains to the estimation error of the pitch angle. So, $z_1 = \hat{y}_1$, $z_2 = \hat{\dot{y}}_1$, $z_7 = \hat{f}_1$, $e_{E1} = \hat{y}_1 - y_1$. The expression of $fal_i\left(e_{E1}, a_i\right)$ is as follows [25]

$$fal_i\left(e_{E1}, a_i\right) = \begin{cases} |e_{E1}|^{a_i} \operatorname{sgn}\left(e_{E1}\right) & |e_{E1}| > \delta \\ \frac{e_{E1}}{\delta^{(1-a_i)}} & |e_{E1}| < \delta \end{cases} \tag{20}$$

where $0 < a_7 < a_2 < a_1 \leq 1$, $0 < \delta < 1$.

To enhance the accuracy of estimation, the ESO typically applies a larger gain for the observer. Nonetheless, augmenting the gain amplifies the noise, consequently undermining the controller's performance. Due to the measurability of the state variables in the attitude system, $e_{E_2} = \hat{\dot{y}}_1 - \dot{y}_1$ is utilised in place of e_{E1} to mitigate the gain and suppress the noise. The design of the RESO is as follows:

$$\begin{cases} \dot{z}_2 = z_7 - \bar{b}_2 fal_2\left(e_{E2}, \bar{a}_2\right) + \nu_1 \\ \dot{z}_7 = -\bar{b}_7 fal_7\left(e_{E2}, \bar{a}_7\right) \end{cases} \tag{21}$$

To rectify the issue of poor control accuracy when the error is large, an enhancement is implemented:

$$fal_i\left(e_{E2}, \bar{a}_i\right) = \begin{cases} |e_{E2}|^{\bar{a}_i} \tanh\left(e_{E2}\right) & |e_{E2}| > \delta \\ \frac{e_{E2}}{\delta^{(1-\bar{a}_i)}} & |e_{E2}| < \delta \end{cases} \tag{22}$$

In contrast to the ESO, the RESO eliminates the need for secondary estimation of known output variable, diminishes the phase lag attributed to the observer and enhances the accuracy of disturbance estimation. Moreover, the proposed observer is characterised by a simple structure, capable of achieving commendable estimation performance with a smaller gain, and effectively reduces the engineering application cost.

3.2 Design of the CNFTSMC

Using the pitch angle channel as an illustration to design the CNFTSMC. The design method for the remaining channels is similar. Let y_{1d} present the desired output, y_1 denote the actual output, and define the system error [26] and its derivative as follows [27]:

$$e_1 = y_1 - y_{1d} \tag{23}$$

$$\dot{e}_1 = \dot{y}_1 - \dot{y}_{1d} \tag{24}$$

$$\ddot{e}_1 = \ddot{y}_1 - \ddot{y}_{1d} \tag{25}$$

Specify the composite sliding surfaces as follows:

$$s_{11} = e_1 + \alpha_1 sig^{\frac{p_1}{q_1}}\left(e_1\right) + \beta_1 sig^{\frac{m_1}{n_1}}\left(\dot{e}_1\right) \tag{26}$$

https://doi.org/10.1017/aer.2024.4 Published online by Cambridge University Press

$$s_{12} = \dot{e}_1 + \alpha_2 e_1 + \beta_2 sig^{w_1}(e_1) \tag{27}$$

where $sig^{\frac{p_1}{q_1}}(e_1) = \text{sgn}(e_1)|e_1|^{\frac{p_1}{q_1}}$, $\alpha_1 > 0$, $\beta_1 > 0$, $\alpha_2 > 0$, $\beta_2 > 0$, $w_1 > 1$, p_1, q_1, m_1, and n_1 are odd numbers, and satisfy $1 < \frac{m_1}{n_1} < \frac{p_1}{q_1} < 2$.

When $|e_1| < b$, take the sliding surface s_{11}; when $|e_1| \geqslant b$, take the sliding surface s_{12}, where $0 < b < 1$.

From Equation (26), it can be inferred that

$$\dot{s}_{11} = \dot{e}_1 \left(1 + \alpha_1 \frac{p_1}{q_1} sig^{\frac{p_1}{q_1}-1}(e_1)\right) + \beta_1 \frac{m_1}{n_1} sig^{\frac{m_1}{n_1}-1}(\dot{e}_1)\ddot{e}_1 \tag{28}$$

By incorporating Equations (17) and (25) into Equation (28), we obtain

$$\dot{s}_{11} = \dot{e}_1 \left(1 + \alpha_1 \frac{p_1}{q_1} sig^{\frac{p_1}{q_1}-1}(e_1)\right) + \beta_1 \frac{m_1}{n_1} sig^{\frac{m_1}{n_1}-1}(\dot{e}_1)(f_1 + \nu_1 - \ddot{y}_{1d}) \tag{29}$$

When the system adheres to the sliding surface, the equivalent control law can be derived as follows:

$$\nu_{1eq} = \ddot{y}_{1d} - f_1 - \frac{n_1}{\beta_1 m_1} sig^{2-\frac{m_1}{n_1}}(\dot{e}_1)\left(1 + \alpha_1 \frac{p_1}{q_1} sig^{\frac{p_1}{q_1}-1}(e_1)\right) \tag{30}$$

Simultaneously, the subsequent switching control law is

$$\nu_{1sw} = -k_1 s_{11} - \eta_1 sgn(s_{11}) \tag{31}$$

where $k_1 > 0$, $\eta_1 > 0$.

Hence, when $|e_1| < b$, the overall control law is

$$\nu_1 = \ddot{y}_{1d} - f_1 - \frac{n_1}{\beta_1 m_1} sig^{2-\frac{m_1}{n_1}}(\dot{e}_1)\left(1 + \alpha_1 \frac{p_1}{q_1} sig^{\frac{p_1}{q_1}-1}(e_1)\right) - k_1 s_{11} - \eta_1 \text{sgn}(s_{11}) \tag{32}$$

From Equation (27), it can be inferred that

$$\dot{s}_{12} = \ddot{e}_1 + \alpha_2 \dot{e}_1 + \beta_2 w_1 sig^{w_1-1}(e_1)\dot{e}_1 \tag{33}$$

By incorporating Equations (17) and (25) into Equation (33), we obtain

$$\dot{s}_{12} = (f_1 + \nu_1 - \ddot{y}_{1d}) + \alpha_2 \dot{e}_1 + \beta_2 w_1 sig^{w_1-1}(e_1)\dot{e}_1 \tag{34}$$

When the system adheres to the sliding surface, the equivalent control law can be derived as follows:

$$\nu_{1eq} = \ddot{y}_{1d} - f_1 - \dot{e}_1 \left(\alpha_2 + \beta_2 w_1 sig^{w_1-1}(e_1)\right) \tag{35}$$

Hence, when $|e_1| \geqslant b$, the overall control law is

$$\nu_1 = \ddot{y}_{1d} - f_1 - \dot{e}_1 \left(\alpha_2 + \beta_2 w_1 sig^{w_1-1}(e_1)\right) - k_1 s_{12} - \eta_1 sgn(s_{12}) \tag{36}$$

It is worth noting that the discontinuity of the sign function $sgn(\cdot)$ in the aforementioned control law can give rise to chattering, which can disrupt actuator performance and excite unmodeled high-frequency dynamic. To mitigate this phenomenon, this paper employs the hyperbolic tangent function $tanh(\cdot)$ instead of the sign function [28]. Specifically, $sgn(s_{11})$ is substituted with $\tanh(s_{11}/\sigma)$, and $sgn(s_{12})$ is substituted with $\tanh(s_{12}/\sigma)$, where σ is a very small positive number.

In summary, when $|e_1| < b$, the composite sliding mode control law based on the RESO is

$$\nu_1 = \ddot{y}_{1d} - \hat{f}_1 - \frac{n_1}{\beta_1 m_1} sig^{2-\frac{m_1}{n_1}}(\dot{e}_1)\left(1 + \alpha_1 \frac{p_1}{q_1} sig^{\frac{p_1}{q_1}-1}(e_1)\right) - k_1 s_{11} - \eta_1 \tanh(s_{11}/\sigma) \tag{37}$$

When $|e_1| \geqslant b$, the composite sliding mode control law based on the RESO is

$$\nu_1 = \ddot{y}_{1d} - \hat{f}_1 - \dot{e}_1 \left(\alpha_2 + \beta_2 w_1 sig^{w_1-1}(e_1)\right) - k_1 s_{12} - \eta_1 \tanh(s_{12}/\sigma) \tag{38}$$

https://doi.org/10.1017/aer.2024.4 Published online by Cambridge University Press

4.0 Stability analysis

4.1 Observer stability analysis

In this section, we take the pitch channel as an example to demonstrate that the proposed improved RESO guarantees bounded estimation error, with analogous analysis applied to the remaining two channels.

Theorem 1. *For the pitch angle channel represented by Equation (17), the estimation error of the proposed improved RESO is bounded.*

Proof. Let $\lambda_i(e_{E2}) = \frac{fal_i(e_{E2},\bar{a}_i)}{e_{E2}}$, $\dot{f}_1 = \varpi$, and define $e_{E3} = \hat{f}_1 - f_1$ as the estimation error of f_1. $e_E = [e_{E2}, e_{E3}]^T$ represents the state error estimation vector. By employing Equation (21), we can deduce the differential equation for e_E

$$\dot{e}_E = A_E e_E - B_E \varpi \tag{39}$$

where $A_E = \begin{bmatrix} -\bar{b}_2\lambda_2(e_{E2},\bar{a}_2)1 \\ -\bar{b}_7\lambda_7(e_{E2},\bar{a}_7)0 \end{bmatrix}$, $B_E = \begin{bmatrix} 0 \\ 1 \end{bmatrix}$

Given that $\bar{b}_2 > 0, \bar{b}_7 > 0, \lambda_2\left(e_{E2},\bar{a}_2\right) > 0, \lambda_7\left(e_{E2},\bar{a}_7\right) > 0, A_E$ can be identified as a Hurwitz matrix. Based on the Hurwitz stability theory [29], it can be inferred that Equation (39) is stable, and e_E is bounded. Consequently, the estimation error of the proposed improved RESO is bounded. □

4.2 Controller stability analysis

In this section, we illustrate the convergence of the tracking error to zero within a finite time and demonstrate that the actual state can track the desired value within a finite time using the pitch channel as an example.

Based on the stability analysis of the observer, it is known that the estimation error of the proposed improved RESO is bounded. Without loss of generality, assume $\left|f_1 - \hat{f}_1\right|_{\max} \le L_1, L_1 < \eta_1$.

Theorem 2. *For system 16, taking the sliding surface 26 and using the control law 37, the attitude tracking error converges to zero within a finite time.*

Proof. When $|e_1| < b$, we select the Lyapunov function as

$$V_{11} = \frac{1}{2}{s_{11}}^2 \tag{40}$$

Differentiating Equation (40) yields

$$\dot{V}_{11} = s_{11}\left(\dot{e}_1\left(1 + \alpha_1\frac{p_1}{q_1}sig^{\frac{p_1}{q_1}-1}(e_1)\right) + \beta_1\frac{m_1}{n_1}sig^{\frac{m_1}{n_1}-1}(\dot{e}_1)(f_1 + \nu_1 - \ddot{y}_{1d})\right) \tag{41}$$

By substituting Equation (37) into Equation (41), we obtain

$$\dot{V}_{11} = \beta_1\frac{m_1}{n_1}sig^{\frac{m_1}{n_1}-1}(\dot{e}_1)\, s_{11}\left(f_1 - \hat{f}_1 - k_1 s_{11} - \eta_1\tanh(s_{11}/\sigma)\right) \tag{42}$$

Since $\left|f_1 - \hat{f}_1\right|_{\max} \le L_1, L_1 < \eta_1$, according to Equation (42), we have

$$\dot{V}_{11} \le -\beta_1\frac{m_1}{n_1}sig^{\frac{m_1}{n_1}-1}(\dot{e}_1)\left(k_1 s_{11}^2 + (\eta_1 - L_1)|s_{11}|\right) \tag{43}$$

Let $\beta_1\frac{m_1}{n_1}sig^{\frac{m_1}{n_1}-1}(\dot{e}_1) = \varepsilon$, since $1 < \frac{m_1}{n_1} < 2$, then $sig^{\frac{m_1}{n_1}-1}(\dot{e}_1) > 0$, and thus $\varepsilon > 0$.
From Equation (43), we obtain

$$\dot{V}_{11} \le -2\varepsilon k_1 V_{11} - \sqrt{2}\varepsilon(\eta_1 - L_1)V_{11}^{\frac{1}{2}} \tag{44}$$

https://doi.org/10.1017/aer.2024.4 Published online by Cambridge University Press

Let $2\varepsilon k_1 = \alpha_3$, $\sqrt{2}\varepsilon\ (\eta_1 - L_1) = \alpha_4$, we have

$$\dot{V}_{11} \leq -\alpha_3 V_{11} - \alpha_4 V_{11}^{\frac{1}{2}} \tag{45}$$

According to Lemma 1, the sliding variable s_{11} converges to zero within a finite time, with the convergence time satisfies

$$\mathrm{T}_1 \leq \frac{2}{\alpha_3} \ln \frac{\alpha_3 V_{11}^{\frac{1}{2}}(0) + \alpha_4}{\alpha_4} \tag{46}$$

Given that the system state reaches the sliding surface s_{11} at $t = t_1$, where $t_1 \leq T_1$, it ensures that when

$$e_1 + \alpha_1 sig^{\frac{p_1}{q_1}}(e_1) + \beta_1 sig^{\frac{m_1}{n_1}}(\dot{e}_1) = 0 \tag{47}$$

From Equation (47), we obtain

$$\dot{e}_1 = -\beta_1^{-\frac{n_1}{m_1}} e_1^{\frac{n_1}{m_1}} \left(1 + \alpha_1 sig^{\frac{p_1}{q_1}-1}(e_1)\right)^{\frac{n_1}{m_1}} \tag{48}$$

Choosing the Lyapunov function as

$$V_{12} = \frac{1}{2} {e_1}^2 \tag{49}$$

Differentiating Equation (49) yields

$$\dot{V}_{12} = e_1 \dot{e}_1 \tag{50}$$

By substituting Equation (48) into Equation (50), we obtain

$$\dot{V}_{12} = -\beta_1^{-\frac{n_1}{m_1}} e_1^{\frac{n_1}{m_1}+1} \left(1 + \alpha_1 sig^{\frac{p_1}{q_1}-1}(e_1)\right)^{\frac{n_1}{m_1}} \tag{51}$$

From Equation 51, we obtain

$$\begin{aligned} \dot{V}_{12} &= -\beta_1^{-\frac{n_1}{m_1}} \sqrt{2}^{\frac{n_1}{m_1}+1} V_{12}^{\frac{n_1+m_1}{2m_1}} \left(1 + \sqrt{2}^{\frac{p_1}{q_1}-1} \alpha_1 V_{12}^{\frac{p_1-q_1}{2q_1}}\right)^{\frac{n_1}{m_1}} \\ &\leq -\beta_1^{-\frac{n_1}{m_1}} \sqrt{2}^{\frac{n_1}{m_1}+1} V_{12}^{\frac{n_1+m_1}{2m_1}} \end{aligned} \tag{52}$$

Let $\beta_1^{-\frac{n_1}{m_1}} \sqrt{2}^{\frac{n_1}{m_1}+1} = \alpha_5$, we have

$$\dot{V}_{12} \leq -\alpha_5 V_{12}^{\frac{n_1+m_1}{2m_1}} \tag{53}$$

According to Lemma 2, the attitude tracking error e_1 converges to zero within a finite time, with the convergence time satisfies

$$\mathrm{T}_2 \leq \frac{2m_1}{\alpha_5 (m_1 - n_1)} V_{12}^{\frac{m_1-n_1}{2m_1}}(0) \tag{54}$$

In conclusion, when $|e_1| < b$, the system is finite-time stable, and the overall convergence time satisfies

$$\mathrm{T} \leq \mathrm{T}_1 + \mathrm{T}_2 \tag{55}$$

□

Theorem 3. *For system 16, taking the sliding surface 27 and using the control law 38, the attitude tracking error converges to zero within a finite time.*

Proof. When $|e_1| \geqslant b$, we select the Lyapunov function as

$$V_{21} = \frac{1}{2} {s_{12}}^2 \tag{56}$$

https://doi.org/10.1017/aer.2024.4 Published online by Cambridge University Press

Table 1. *Model parameters*

Parameter	Value
m (kg)	329
I_x $(\mathrm{kg}\cdot\mathrm{m}^2)$	833.222
I_y $(\mathrm{kg}\cdot\mathrm{m}^2)$	13,229.52
I_z $(\mathrm{kg}\cdot\mathrm{m}^2)$	12,856.753
I_{xz} $(\mathrm{kg}\cdot\mathrm{m}^2)$	1,047.665
z_G (m)	0.902

Table 2. *External disturbances*

External disturbance torque	$t < 150$	$150 \le t \le 180$	$t > 180$
d_1 (N)	0	600	600+300sin(0.1t)
d_2 (N)	0	400	−400−200sin(0.1t)
d_3 (N)	0	400	400+200sin(0.1t)

Differentiating Equation (56) yields

$$\dot{V}_{21} = s_{12}\left(f_1 + v_1 - \ddot{y}_{1d} + \dot{e}_1\left(\alpha_2 + \beta_2 w_1 sig^{w_1-1}(e_1)\right)\right) \tag{57}$$

By substituting Equation (38) into Equation (57), we obtain

$$\dot{V}_{21} = s_{12}\left(f_1 - \hat{f}_1 - k_1 s_{12} - \eta_1 \tanh\left(s_{12}/\sigma\right)\right) \tag{58}$$

Since $\left|f_1 - \hat{f}_1\right|_{\max} \le L_1$, $L_1 < \eta_1$, according to Equation (58), we have

$$\dot{V}_{21} \le -k_1 {s_{12}}^2 - (\eta_1 - L_1)\,|s_{12}| \tag{59}$$

From Equation (59), obtain

$$\dot{V}_{21} \le -2k_1 V_{21} - \sqrt{2}\,(\eta_1 - L_1)\,{V_{21}}^{\frac{1}{2}} \tag{60}$$

Let $2k_1 = \alpha_6$, $\sqrt{2}\,(\eta_1 - L_1) = \alpha_7$, we have

$$\dot{V}_{21} \le -\alpha_6 V_{21} - \alpha_7 {V_{21}}^{\frac{1}{2}} \tag{61}$$

According to Lemma 1, the sliding variable s_{12} converges to zero within a finite time, with the convergence time satisfies

$$\mathrm{T}_3 \le \frac{2}{\alpha_6}\ln\frac{\alpha_6 V_{21}^{\frac{1}{2}}(0) + \alpha_7}{\alpha_7} \tag{62}$$

In conclusion, when $|e_1| \geqslant b$, the system is finite-time stable, and the overall convergence time satisfies

$$\mathrm{T} \le \mathrm{T}_1 + \mathrm{T}_2 + \mathrm{T}_3 \tag{63}$$

□

5.0 Simulation analysis

5.1 Simulation setup

To validate the effectiveness and superiority of the proposed algorithm, this section conducts two parts of comparative experiments on the decoupled subsystems of pitch, yaw and roll. Firstly, a comparison

https://doi.org/10.1017/aer.2024.4 Published online by Cambridge University Press

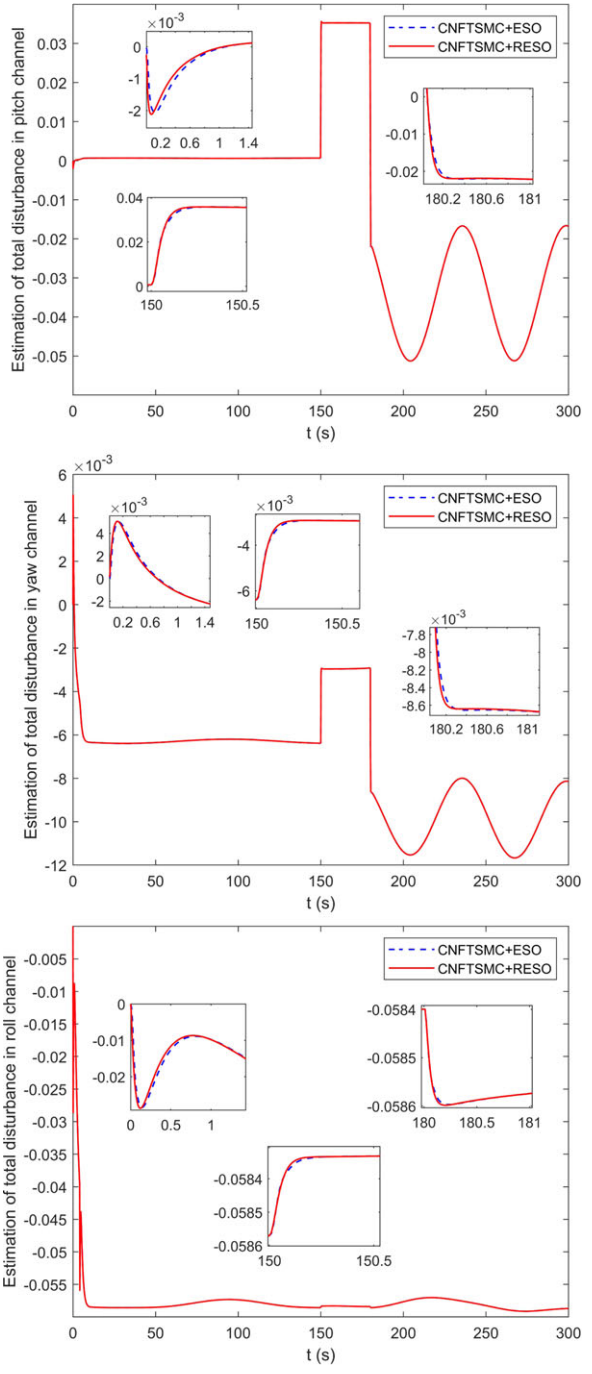

Figure 3. *Estimation of total disturbance under two observers.*

simulation is carried out between the Composite Non-singular Fast Terminal Sliding Mode Control algorithm with the traditional Nonlinear Extended State Observer (CNFTSMC+ESO) and the Composite Non-singular Fast Terminal Sliding Mode Control algorithm with the Reduced-order Extended State Observer (CNFTSMC+RESO). Secondly, a comparison simulation is conducted among the Composite Non-singular Fast Terminal Sliding Mode Control algorithm with the Reduced-order

https://doi.org/10.1017/aer.2024.4 Published online by Cambridge University Press

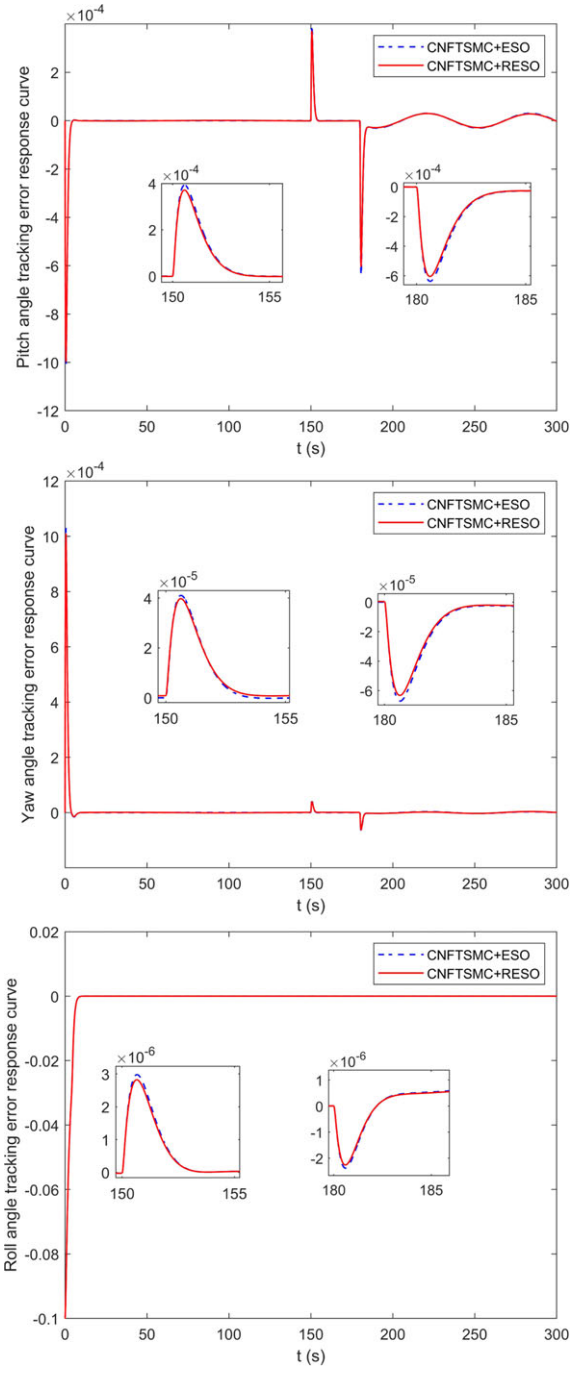

Figure 4. *Attitude angle tracking error response curves under two observers.*

Extended State Observer (CNFTSMC+RESO), the Non-singular Fast Terminal Sliding Mode Control algorithm with the Reduced-order Extended State Observer (NFTSMC+RESO), and the method in (30) with the Reduced-order Extended State Observer (The method in (30)+RESO). Furthermore, the method in Ref. [30] is identical to the method in Ref. [31]. The experimental airship described in Refs (32, 33) serves as the research object, with the primary model parameters shown in Table 1.

https://doi.org/10.1017/aer.2024.4 Published online by Cambridge University Press

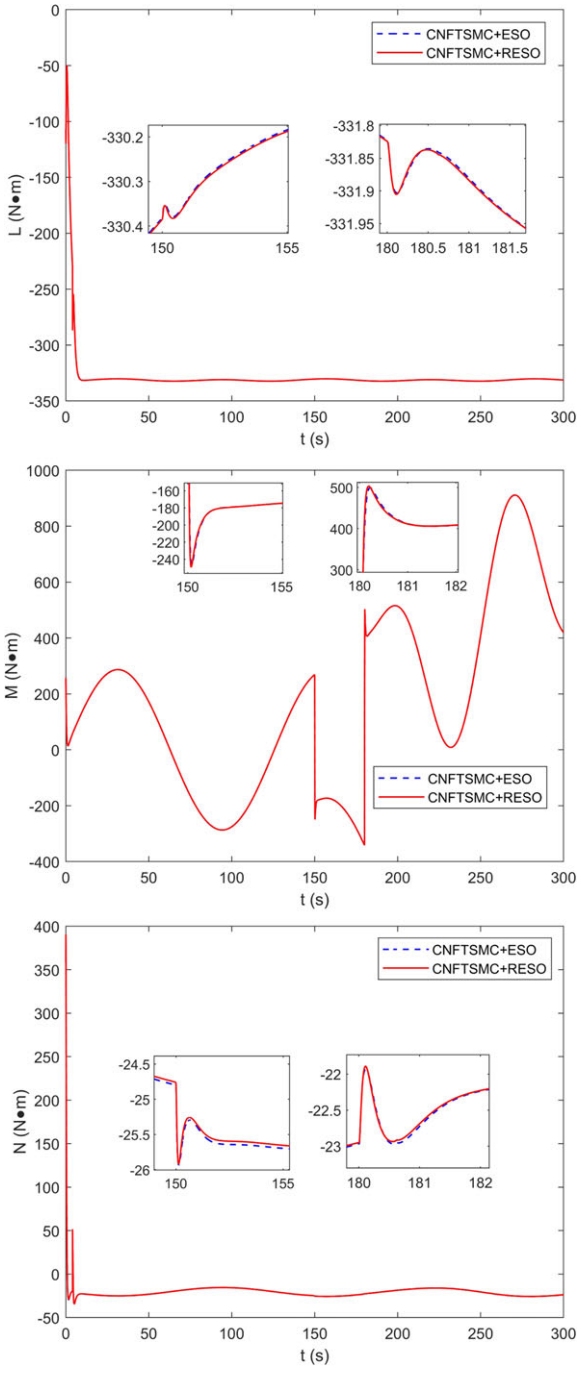

Figure 5. *Control moment response curves under two observers.*

The initial values of the airship attitude system are set as $\theta\ (0) = 0$, $\psi\ (0) = 0$, $\phi\ (0) = 0$, $p\ (0) = 0$, $q\ (0) = 0$, $r\ (0) = 0$. The desired values for pitch, yaw and roll are set as $\theta_d = 0.1\sin(0.05t)$, $\psi_d = -0.1\sin(0.05t)$, $\phi_d = 0.1$. The model parameter perturbations are set as $\Delta I_x = 0.2I_x$, $\Delta I_y = 0.15I_y$, $\Delta I_z = 0.15I_z$, $\Delta I_{xz} = 0.2I_{xz}$. The external disturbances applied to the system dynamics are specified in Table 2.

https://doi.org/10.1017/aer.2024.4 Published online by Cambridge University Press

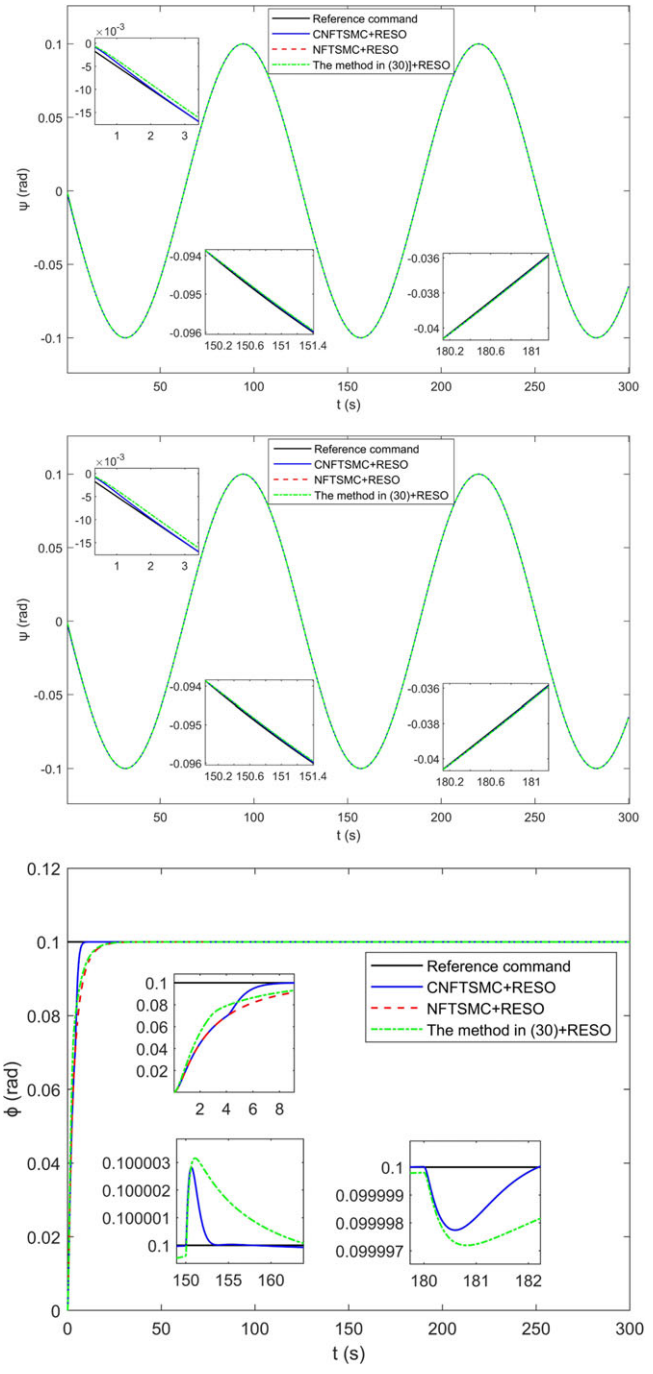

Figure 6. *Attitude angle tracking response curves.*

Taking the pitch channel as an example, the sliding surface design for the NFTSMC+RESO is given by

$$s_{12} = \dot{e}_1 + \alpha_2 e_1 + \beta_2 sig^{w_1}(e_1) \tag{64}$$

The comparative controller design is as follows:

https://doi.org/10.1017/aer.2024.4 Published online by Cambridge University Press

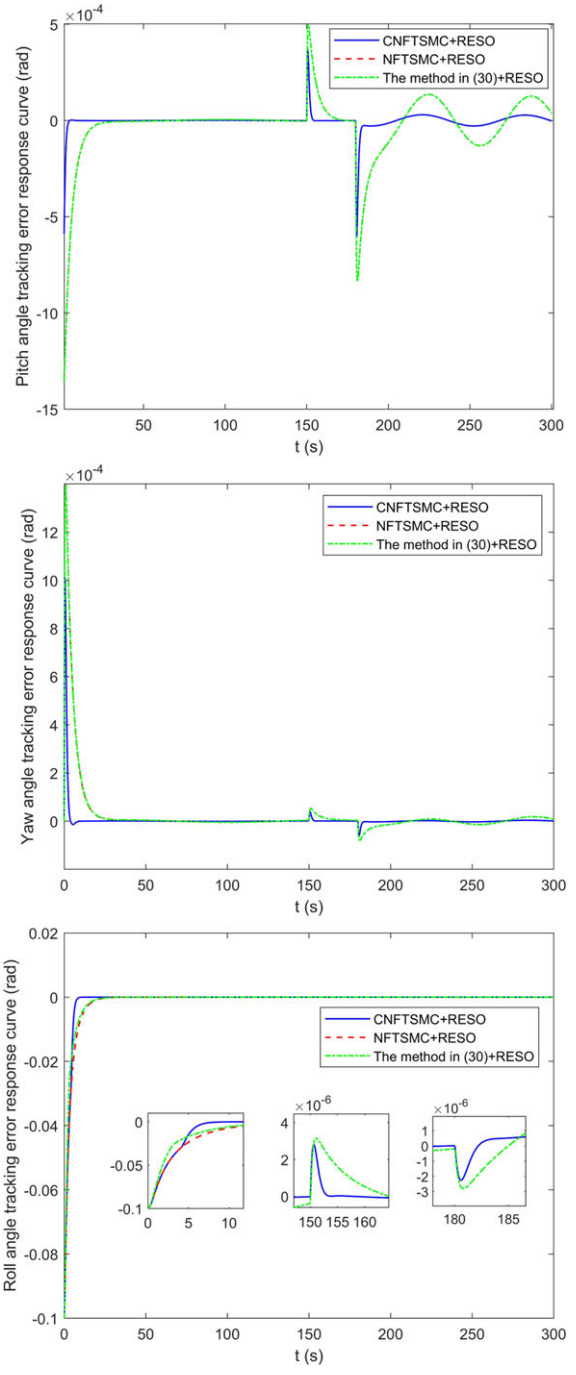

Figure 7. *Attitude angle tracking error response curves.*

$$v_1 = \ddot{y}_{1d} - \hat{f}_1 - \dot{e}_1 \left(\alpha_2 + \beta_2 w_1 sig^{w_1 - 1}(e_1)\right) - k_1 s_{12} - \eta_1 \tanh(s_{12}/\sigma) \tag{65}$$

To ensure fairness, the selection of parameters adheres to three principles [34]: effective control, uniform variables and moderate control variable values. Taking the pitch channel as an example, the simulation parameters for the remaining two channels are consistent with the pitch channel.

https://doi.org/10.1017/aer.2024.4 Published online by Cambridge University Press

Table 3. *Maximum absolute error (***max** $|e|$*)*

Control channel	CNFTSMC+RESO (rad)	NFTSMC+RESO (rad)	The method in (30)+RESO (rad)
Pitch	0.0010	0.0014	0.0014
Yaw	0.0010	0.0014	0.0014
Roll	0.1	0.1	0.1

Table 4. *Mean absolute error (*$\frac{\sum |e|}{N}$*)*

Control channel	CNFTSMC+RESO (rad)	NFTSMC+RESO (rad)	The method in (30)+RESO (rad)
Pitch	1.8×10^{-4}	8.7×10^{-4}	8.7×10^{-4}
Yaw	6.6×10^{-5}	3.3×10^{-4}	3.3×10^{-4}
Roll	0.0092	0.0122	0.0102

Table 5. *Absolute error standard deviation (*$\sqrt{\frac{1}{N}\sum(|e| - \frac{1}{N}\sum|e|)^2}$*)*

Control channel	CNFTSMC+RESO (rad)	NFTSMC+RESO (rad)	The method in (30)+RESO (rad)
Pitch	7.1×10^{-5}	1.7×10^{-4}	1.7×10^{-4}
Yaw	5.8×10^{-5}	1.4×10^{-4}	1.4×10^{-4}
Roll	0.0075	0.0077	0.0077

Table 6. *Integral absolute error (*$\int_0^t |e|dt$*)*

Control channel	CNFTSMC+RESO (rad)	NFTSMC+RESO (rad)	The method in (30)+RESO (rad)
Pitch	0.0053	0.0260	0.0260
Yaw	0.0020	0.0098	0.0099
Roll	0.2768	0.3667	0.3052

The observer parameter values are as follows:

(1) ESO: $a_1 = 1$, $a_2 = 0.5$, $a_7 = 0.25$, $b_1 = 100$, $b_2 = 1,000$, $b_3 = 6,000$, $\delta = 0.01$.
(2) RESO: $\bar{a}_2 = 1$, $\bar{a}_7 = 0.5$, $\bar{a}_2 = 100$, $\bar{a}_7 = 200$, $\delta = 0.01$.

The simulation parameter values for the controllers are as follows:

(1) CNFTSMC: $b = 0.03$, $\alpha_1 = 0.2$, $\beta_1 = 1.5$, $\alpha_2 = 0.2$, $\beta_2 = 1.5$, $p_1 = 5$, $q_1 = 3$, $m_1 = 57$, $n_1 = 55$, $w_1 = 2$, $\sigma = 1$, $\eta_1 = 0.08$, $k_1 = 2$.
(2) NFTSMC: $\alpha_2 = 0.2$, $\beta_2 = 1.5$, $w_1 = 2$, $\sigma = 1$, $\eta_1 = 0.08$, $k_1 = 2$.

5.2 Simulation results analysis

Figure 3 depicts the estimation response of the two observers to the total disturbances under the CNFTSMC. It is evident that the proposed improved RESO exhibits a more rapid and accurate estimation of the disturbances, thereby mitigating the phase lag induced by the observer. In addition, the tracking error and control input of the two comparative observers are illustrated in Figs. 4 and 5. It is

https://doi.org/10.1017/aer.2024.4 Published online by Cambridge University Press

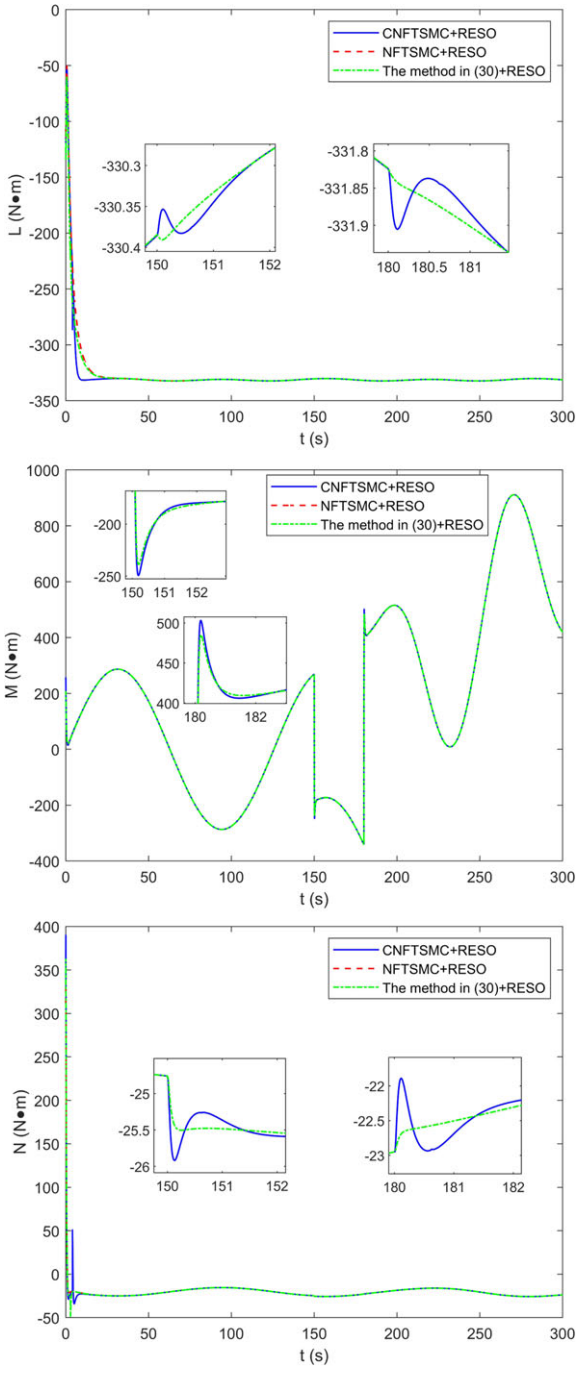

Figure 8. *Control moment response curves.*

apparent that, for the three channels with uniform control input, the tracking error based on the improved RESO is inferior to that based on the ESO, verifying the effectiveness of the proposed observer.

Figure 6 presents the attitude angle tracking response curves for three control methods. It is apparent that the proposed CNFTSMC+RESO, NFTSMC+RESO, and the method in (30)+RESO

https://doi.org/10.1017/aer.2024.4 Published online by Cambridge University Press

adeptly compensate for the disturbances and parameter perturbations by utilising estimation information. Consequently, they achieve precise tracking of the pitch, yaw and roll angle commands in a multiple-disturbances environment.

Figure 7 illustrates the attitude angle tracking error response curves for three control methods. We conduct a comparative analysis with regard to their convergence speed and disturbance rejection capability. It is evident that prior to 150s, in the absence of external disturbances, CNFTSMC+RESO demonstrates a faster convergence speed in the pitch and yaw channels compared to NFTSMC+RESO and the method in (30)+RESO. In the roll channel, when the tracking error is greater than or equal to 0.03, CNFTSMC+RESO and NFTSMC+RESO exhibit the same convergence speed, while the method in (30)+RESO achieves a faster convergence speed compared to the other two methods. When the tracking error falls below 0.03, the convergence speed of CNFTSMC+RESO surpasses that of NFTSMC+RESO and the method in (30)+RESO.

It is noteworthy that the method in (30)+RESO exhibits the advantage of a faster convergence speed when the tracking error is larger, and additionally, this study also evaluates the disturbance rejection capability. Between 150s and 180s, when exposed to constant disturbances, or at 180s when confronted with time-varying disturbances, the attitude angle tracking response under CNFTSMC+RESO exhibits a more rapid recovery, resulting in a shorter adjustment time compared to the other two control methods.

Furthermore, in order to comprehensively compare the performance of the control methods, this section introduces performance indicators for tracking errors, which include the maximum absolute error, average absolute error, absolute error standard deviation and integral absolute error [35]. The control performance indicators for attitude tracking errors under the three control methods are shown in Tables 3, 4, 5 and 6. It can be observed that the proposed CNFTSMC+RESO method attains superior control performance indicators in terms of tracking errors, validating the effectiveness and superiority of the proposed control algorithm.

In conclusion, the CNFTSMC+RESO method demonstrates smaller maximum absolute error, average absolute error, absolute error standard deviation and integral absolute error in comparison to NFTSMC+RESO and the method in (30)+RESO. Additionally, it showcases faster convergence speed and stronger capability for suppressing disturbances.

Figure 8 displays the control torque response curves for the three control methods. By utilising hyperbolic tangent function instead of the sign function in the design of the sliding mode controller, all three control algorithms ensure the continuity of the control quantity. From the figure, it can be observed that the control quantities of the three control algorithms are of equivalent magnitude, indicating that they provide comparable control energy required to achieve the control objectives.

6.0 Conclusion

In summary, this paper addresses the attitude control problem of stratospheric airship in the presence of multiple disturbances. A CNFTSMC scheme based on RESO has been proposed to effectively mitigate the impact of parameter perturbations and external disturbances, thereby enhancing control performance. The effectiveness and superiority of the proposed control method have been substantiated through simulation experiments. The simulation results demonstrate that the proposed control scheme ensures precise tracking of the airship's attitude, significantly improves the response speed, and enhances the anti-interference ability of the attitude tracking.

Furthermore, the control of airship attitude necessitates consideration of the actuators configuration. In future research, we intend to conduct a comprehensive investigation into the manipulation of the airship's actuators, such as propeller vectoring and control of the airship's aerodynamic control surfaces.

Acknowledgements. This work was funded by Natural Science Foundation of China (No. U23A20336, No. 52227811 and No. 61733017).

References

[1] Yao, S.Y. *Research on Modeling and Control of Stratospheric Airship*, Nanjing University of Science and Technology, 2019.
[2] Zhao, Z.H., Li, T., Jiang, B. and Cao, D. Composite continuous fast nonsingular terminal sliding mode control for quadrotor UAV attitude systems, *Control Theory Appl.*, 2023, **40**, (3), pp 459–467.
[3] Sun, L.R., Sun, K.W., Guo, X., Yuan J.C. and Zhu, M. Prescribed-time error-constrained moving path following control for a stratospheric airship with disturbances, *Acta Astronaut.*, 2023, **212**, pp 118.
[4] Yuan, J., Guo, X., Zheng, Z.W., Zhu, M. and Gou, H.B. Error-constrained fixed-time trajectory tracking control for a stratospheric airship with disturbances, *Aerosp. Sci. Technol.*, 2021, pp 118.
[5] Wu, Y., Wang, Q., Duan, D., Xie, W. and Wei, Y. Neuroadaptive output-feedback trajectory tracking control for a stratospheric airship with prescribed performance, *Aeronaut. J.*, 2020, **124**, pp 1–24.
[6] Habibi, H., Safaei, A., Voos, H., Darouach, M. and Sanchez-Lopez, J.L. Safe navigation of a quadrotor UAV with uncertain dynamics and guaranteed collision avoidance using barrier Lyapunov function, *Aerosp. Sci. Technol.*, 2023, **132**.
[7] Wu, G., Lin, B.J. and Zhang, S. Fault-tolerant backstepping attitude control for autonomous airship with sensor failure, *Proc. Eng.*, 2012, **29**, pp 2022–2027.
[8] Wang, H., and Li, Z.B. The simulation for the attitude stability control of the stratosphere airship, *Comput. Simul.*, 2018, **35**, (6), pp 55–59+416.
[9] Le, R.C., Wang, X.L., Duan, D.P., and Wu, Y. Attitude control strategy of airship based on active disturbance rejection controller, *Aerosp. Syst.*, 2021, **4**, (1), pp 2022–2027.
[10] Ding, S.H., Levant, A. and Li, S.H. Simple homogeneous sliding-mode controller, *Automatica*, 2016, **67**, pp 22–32.
[11] Shao, X.Y., Sun, G.H., Xue, C. and Li, X.L. Nonsingular terminal sliding mode control for free-floating space manipulator with disturbance, *Acta Astronaut.*, 2021, pp 396–404.
[12] Yang, Y.N., Wu, J. and Zheng, W. Terminal sliding mode control for attitude tracking of autonomous airship, *Chin. Space Sci. Technol.*, 2012, **32**, (4), pp 29–36.
[13] Razmjooei, H., Palli, G. and Abdi, E. Continuous finite-time extended state observer design for electro-hydraulic systems, *J. Franklin Institute*, 2022, **359**, pp 5036–5055.
[14] Wang, G.L., Liu, R., Zhao, N.N., Ding, D.W. and Xu, D.G. Enhanced linear ADRC strategy for HF pulse voltage signal injection-based sensorless IPMSM drives, *IEEE Trans. Power Electron.*, 2019, **34**, (1), pp 514–525.
[15] Chen, B.W. *Research on Flight Motion Control of a Stratospheric Airship*, Amoy University, 2018.
[16] Fu, C.F. and Tan, W. Analysis and tuning of reduced-order active disturbance rejection control, *J. Franklin Inst.*, 2021, **358**, (1), pp 339–362.
[17] Wang, Y.Y., Zhou, P.F., Chen, J.A. and Duan, D.P. Finite time attitude tracking control of an autonomous airship, *Trans. Inst. Meas. Control*, 2018, **40**, (1), pp 155–162.
[18] Yang, Y.Y. *Dynamics Modeling and Flight Control for a Stratospheric Airship*, National University of Defense Technology, 2013.
[19] Yang, P., Su, Y.X. and Zhang, L.Y. Proximate fixed-time fault-tolerant tracking control for robot manipulators with prescribed performance, *Automatica*, 2023, **157**.
[20] Mu, D.D., Li, L., Wang, G.F., Fan, Y.S., Zhao, Y.S. and Sun, X.J. State constrained control strategy for unmanned surface vehicle trajectory tracking based on improved barrier Lyapunov function, *Ocean Eng.*, 2023, **277**.
[21] Wang, N., Deng, Q., Xie, G.M. and Pan, X.X. Hybrid finite-time trajectory tracking control of a quadrotor, *ISA Trans.*, 2019, **90**, pp 278–286.
[22] Ou, Y.J. *Research on Modeling and Control Method of Unmanned Airship in the Air*, Shanghai Jiao Tong University, 2003.
[23] Ghadiri, H., Emami, M. and Khodadadi, H. Adaptive super-twisting non-singular terminal sliding mode control for tracking of quadrotor with bounded disturbances, *Aerosp. Sci. Technol.*, 2021, **112**.
[24] Zhai, J., Li, S.Q., Xu, Z., Zhang, L.Y. and Li, J. Reduced-order extended state observer-based sliding mode control for all-clamped plate using an inertial actuator, *Energies*, 2022, **15**.
[25] Wang, X.P., Yao, S.Y. and Qu, C.Y. Direct thrust force control of primary permanent magnet linear motor based on improved extended state observer and model-free adaptive predictive control, *Actuators*, 2022, **11**, (10).
[26] Jahanshahi, H., Yao, Q.J, Khan, M. and Moroz, I. Unified neural output-constrained control for space manipulator using tan-type barrier Lyapunov function, *Adv. Space Res.*, 2023, **71**, pp 3712–3722.
[27] Chen, Q., Yang, Z.X. and Fu, Z.M. RBF nonsingular fast terminal sliding mode tracking control for piezoelectric positioning stage, *J. Henan Univ. Sci. Technol. (Nat. Sci.)*, 2021, **42**, (1), pp 20–26+3.
[28] Aghababa, M.P. and Akbari, M.E. A chattering-free robust adaptive sliding mode controller for synchronization of two different chaotic systems with unknown uncertainties and external disturbances, *Appl. Math. Comput.*, 2012, **218**, (9), pp 5757–5768.
[29] Yao, J.Y. and Deng, W.X. Active disturbance rejection adaptive control of hydraulic servo systems, *IEEE Trans. Ind. Electron.*, 2017, **64**, (10), pp 8023–8032.
[30] Derrouaoui, S.H., Bouzid, Y., Belmouhoub, A. and Guiatni, M. Improved robust control of a new morphing quadrotor UAV subject to aerial configuration change, *Unmanned Syst.*, 2023.
[31] Derrouaoui, S.H., Bouzid, Y., Belmouhoub, A. and Guiatni, M. Enhanced nonlinear adaptive control of a novel over-actuated reconfigurable quadcopte, In 2023 *International Conference on Unmanned Aircraft Systems*, 2023, pp 229-234.
[32] Wang, X.L. *The Study of Nonlinear Aerodynamics and Motion of Stratosphere Earth Observation Platform*, Shanghai Jiao Tong University, 2006.
[33] Wang, X.L. and Shan, X.X. Study of robust control for stratosphere airship attitude, *J. Syst. Simul.*, 2006, **18**, (5).

https://doi.org/10.1017/aer.2024.4 Published online by Cambridge University Press

[34] Sha, L., Wang, S.B. and Liu, Y.J. Nonsingular fast terminal sliding mode control based on extended state observer for two mass systems, *Control Decis.*, 2023, **38**, (3), pp 850–856.
[35] Zhang, Z., Guo, Y.N., Gong, D.W., Zhu, S. and Tian, B. Sliding mode swing angle control for a hydraulic roofbolter based on improved extended state observer, *Acta Automat. Sin.*, 2023, **49**, (6), pp 1256–1271.

Cite this article: Li Z.B., He D.P., Zhang J.Q. and Meng X.R. (2024). Finite-time attitude tracking control of stratospheric airship in the presence of multiple disturbances. *The Aeronautical Journal*, **128**, 2126–2147. https://doi.org/10.1017/aer.2024.4